

Large-Area Aminated-Graphdiyne Thin Films for Direct Methanol Fuel Cells

HPSTAR
834-2019

Fan Wang, Zicheng Zuo,* Liang Li, Kuo Li, Feng He, Zhongqing Jiang,* and Yuliang Li*

Abstract: A two-dimensional (2D) carbon nanofilm with uniform artificial nanopores is an ideal material to ultimately suppress the fuel permeation in the proton exchange membrane fuel cells. Graphdiyne has great mechanical strength, high dimensional stability, and controllable nanopores, and has good prospects to play this crucial role. It is found that graphdiyne nanofilm with amino groups and natural nanopores can be easily prepared with high integrity. The aminated graphdiyne has good compatibility with the Nafion matrix owing to the acid–base interaction between them. The excellent comprehensive properties of graphdiyne in selectivity, dimensional stability, and integrity effectively improve the power performance and stability of fuel cells at wide temperature. Our results can be developed into a universal method that can easily realize the selective separation of ions and small molecules, and open a new way for the emerging applications in green energy.

The direct methanol fuel cell (DMFC) has been highly concerned as one of the promising power supplies,^[1] because of its advantages in terms of portability, safety, high energy density, and renewability.^[2] Nafion membrane is still the benchmark of proton exchange membrane (PEM), because of its high proton conductivity and stability.^[3] However, its high proton conductivity is also accompanied by serious methanol permeability,^[3] which reduces the utilization efficiency of methanol, and poisons the cathode catalysts. Its essence is the unstable and widely-distributed ionic cluster in Nafion^[4] under different temperatures.^[2b] Scientists have focused on solving this problem for decades. They have tried to add

crosslinking additives and pore blockers.^[2b,5] Among them, the utilization of 2D materials (graphene, h-BN) with nanopores are promising owing to the good dimensional stability.^[6] However, the limitations in the preparation and perforation technologies prevent us to achieve large-scale 2D material with uniform nanopores for DMFCs.^[7]

From the perspective of structure, 2D atomic crystal graphdiyne (GDY) shows unique advantages in term of selective nanopores, dimensional stability, and preparation.^[8] GDY has already shown strong potential in the energy storage, catalysis, and optoelectronics.^[9] It theoretically shows high selectivity in seawater desalination and fuel and gas separation.^[10] GDY possesses 2D conjugated skeleton, and therefore the in-plane pores can inherently maintain outstanding dimensional stability in a wide temperature range. Its combination with Nafion can produce an ideal membrane with complementary advantages in proton conductivity and methanol suppression. However, the preparation of single-layer and double-layer GDY films with selective transfer is still a scientific challenge.

To achieve the molecular selectivity in any thickness and good compatibility with Nafion, an aminated GDY (named as NH₂-GDY) nanofilm with well-ordered structure is prepared in large scale. The intrinsic nanopores in NH₂-GDY are large enough to ensure the selective accessibility of proton in any thickness, and the amino groups increase the compatibility owing to the acid–base interaction with Nafion. Its combination with Nafion greatly suppresses the methanol crossover, and enhances the performance in DMFCs. This work detours the challenges in the perforation technology and thin carbon film preparation, and it shows a great universality for readily constructing the 2D porous carbon nanofilm with high selectivity for many applications.

The structure and synthesis process of NH₂-GDY are shown in the Supporting Information, Figures S1–S6. The NH₂-GDY can be largely synthesized via the state-of-the-art method (Supporting Information, Figure S7).^[11] After the removal of Cu foil, the NH₂-GDY film maintains a good integrity, and it is transparent (Supporting Information, Figure S7a,b). The good continuity is beneficial for the selective transfer of proton and preventing the methanol crossover. It is strong enough to be transferred easily into the Nafion solution for the membrane preparation of NH₂-GDY@Nafion, and no cracks are appeared (Supporting Information, Figure S7c,d). The NH₂-GDY is successfully embedded in the Nafion matrix (Supporting Information, Figure S7d). The Raman spectrometer is widely applied in the characterization of carbon materials owing to their strong characteristic peaks.^[12] The strong peak over 2150 cm⁻¹ is originated from the stretching vibrations of the diyne linkage

[*] F. Wang, Prof. Z. Zuo, L. Li, Dr. F. He, Prof. Y. Li
Beijing National Laboratory for Molecular Sciences (BNLMS), CAS
Research/Education Center for Excellence in Molecular Sciences,
Institute of Chemistry, Chinese Academy of Sciences
Beijing 100190 (P. R. China)
E-mail: zuozic@iccas.ac.cn
ylli@iccas.ac.cn

F. Wang, L. Li, Prof. Y. Li
Department of Chemistry, University of Chinese Academy of Sciences
Beijing 100049 (P. R. China)

Prof. K. Li
Center for High Pressure Science and Technology Advanced Research
Beijing 100049 (P. R. China)

Prof. Z. Jiang
Key Laboratory of Optical Field Manipulation of Zhejiang Province
Department of Physics, Zhejiang Sci-Tech University
Hangzhou 310018 (P. R. China)
E-mail: zhongqingjiang@zstu.edu.cn

Supporting information and the ORCID identification number(s) for the author(s) of this article can be found under:
<https://doi.org/10.1002/anie.201910588>.

(Supporting Information, Figure S8), indicating that the NH_2 -GDY is high quality. The high-quality of NH_2 -GDY is also confirmed by the IR spectroscopy in the Supporting Information, Figure S9. The solid-state ^{13}C -NMR (Supporting Information, Figure S10) shows the characteristic of carbon elements in the NH_2 -GDY, and C configurations are well coincident with the structure of NH_2 -GDY. Also, the peaks of the corresponding elements in XPS (Supporting Information, Figure S11) can be well-deconvoluted and assigned to the accurate structure of the NH_2 -GDY. According to these measurements, it can be concluded that the NH_2 -GDY with well-defined structure is prepared. The XRD testing (Supporting Information, Figure S12) has a strong peak at a 2θ of 24° , corresponding to the interlayer distance of 2D NH_2 -GDY, similar to other 2D carbon materials.^[13]

In the SEM (Figure 1 a; Supporting Information, Figure S13), it can be seen that the large-scale NH_2 -GDY film has good connectivity and flexibility. AFM (Figure 1 b; Supporting Information, Figure S14) shows that such a film is smooth with a thickness of about 13.8 nm. The TEM image (Figure 1 c; Supporting Information, Figure S15) exhibits the good flexibility and uniformity of NH_2 -GDY. The uniform feature and large-scale integrity are necessary to realize stable selectivity for the methanol suppression in the DMFC. The elemental distributions (Supporting Information, Figure S16) ambiguously reveal the carbon-rich nature of NH_2 -GDY with well-distributed N elements. The interlayer distance is 0.36 nm (Supporting Information, Figure S15b). Its well-ordered structure is observed as shown in Figure 1 d,e. The typical characteristic lattice fringes with an interval of 0.47 nm

can be clearly seen (Figure 1 d,e), and the high-quality electron diffraction can be obtained (Figure 1 f). Because NH_2 -GDY has a 2D hexagonal lattice with $a = 1.66$ nm, the SAED was also indexed using a lattice with $a = 1.66$ nm, with the spots close to the direct beam indexed as 300 and its equivalents (Figure 1 f).

The absence of $hk0$ ($h, k < 3$) was attributed to the symmetric extinction and intensity extinction, which suggests a $1/3 \times 1/3$ hexagonal lattice on the 2D projection, with $a = 0.55$ nm, which is $2/\sqrt{3}$ times of the 0.47 nm interval and $\sqrt{3}/3$ times of the edge of the hexagonal ring. Hence we proposed a stacking model of NH_2 -GDY, as shown in Figure 1 g,h. One NH_2 -GDY layer is shifted by $1/3a$ (or its equivalent direction) compared to its neighbors. On the 2D projection, the benzene rings are located next to the center of the diyne groups of its projection of the neighboring layers, and the projection of all of the benzene rings forms the hexagonal lattice of $a = 0.55$ nm. To simulate a perfect SAED pattern, a 9-layer model is needed. In practice, some disordered stacking may present and will not affect the SAED pattern. Therefore, the possible disorder may produce two stacking models with the largest (hexagonal) and the smallest (rhombus) pores as shown in Figure 1 i–l. The size of both pores is enough for proton cross-plane transfer. Owing to the presence of amino groups, two kinds of proton transfer mechanisms will possibly happen, as illustrated in Figure 1 m and the Supporting Information, Figure S17. The Grotthuss-type transfer is taken place among the adjacent amino groups,^[14] and the vehicle type transfer is the dominated approach when their distance becomes larger. In the Grotthuss-type model, the

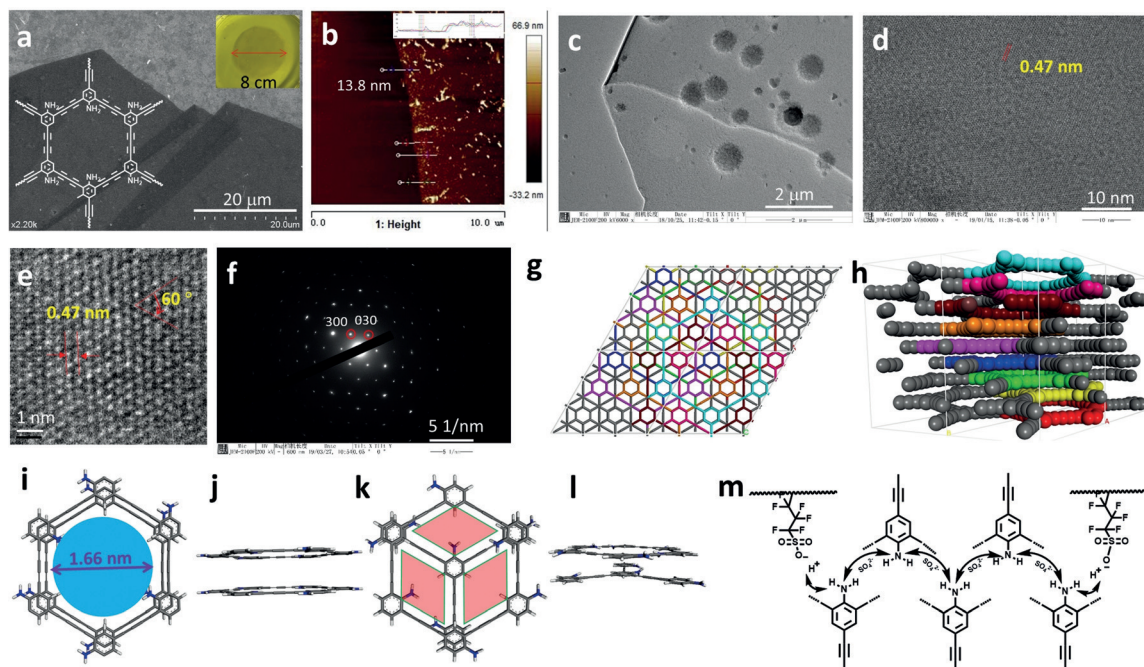


Figure 1. Characterization of NH_2 -GDY. a) SEM image, b) AFM image with the corresponding height, and c) TEM image of NH_2 -GDY film; d) well-defined pattern of NH_2 -GDY; e) the ABSF-filtered image in (d); f) selected-area electron diffraction (SAED); g) structural simulation of NH_2 -GDY; h) the stacking property of multilayer NH_2 -GDY; the different colors show the transfer channel for protons; i) and j) the AA stacking with the widest hexagonal pores; k) and l) the AB stacking with the narrowest rhombus pores; m) the vehicle-type mechanism of the proton transfer among interlayers in the NH_2 -GDY membrane.

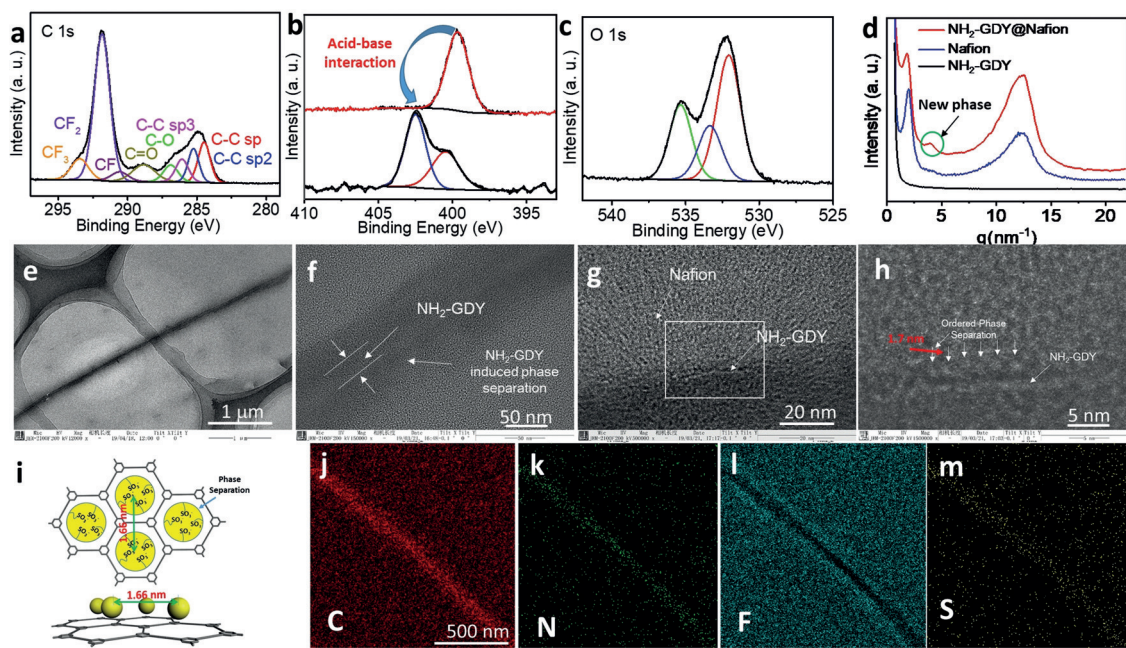


Figure 2. Interaction between Nafion and $\text{NH}_2\text{-GDY}$. a)–c) High-resolution XPS spectra of the composition membrane; d) One-dimensional grazing incident X-ray diffraction plots (1D-GIXRD) of samples. e) Large-scale TEM image of the $\text{NH}_2\text{-GDY}$ film embedded in the Nafion; f) magnified image showing the induced phase separation of Nafion; g) magnified image exhibiting the profiles of $\text{NH}_2\text{-GDY}$ in the Nafion; h) high-resolution TEM image near the surface of the $\text{NH}_2\text{-GDY}$; i) the possible assemble of Nafion on the $\text{NH}_2\text{-GDY}$; j)–m) the element distribution near the $\text{NH}_2\text{-GDY}$ film.

protons jump between the hydrogen bonds and/or the proton passes down the chain of water molecules in which the process of continuous generation and decomposition of the hydrogen bond is carried out. It is considered to be efficient for the selective transfer.^[15] The vehicle mechanism is that the protons and medium (here H_2O) are combined into larger particles (for example, $\text{H}^+(\text{H}_2\text{O})_n$) to diffuse in the electrolyte.

The XPS and GIXRD were used to verify the interaction between $\text{NH}_2\text{-GDY}$ and Nafion (Figure 2; Supporting Information, Figure S18, S19). The high-resolution XPS of C 1s shows the composition of such membrane (Figure 2a). According to our design, the amino groups in $\text{NH}_2\text{-GDY}$ are to tune the assembly of Nafion. Figure 2b reveals that the binding energy of N1s shifts from 400 eV to 402.5 eV. It can be fitted well into two peaks, which is of the amino groups and its protonated forms. The protonated amino group is the indication that the acid-base interaction between the Nafion and $\text{NH}_2\text{-GDY}$ is present, and two proton transfer mechanisms will happen. Such strong acid–base interaction will greatly impact the phase separation of Nafion by tuning the counter-balance between the electrostatic energy and the deformation of backbone chains.^[16] The variations in O 1s are due to the introduction of Nafion (Figure 2c; Supporting Information, Figure S11 d). The microstructure of the membranes was then analyzed by GIXRD (Figure 2d; Supporting Information, Figure S19). In Figure 2d, the broad peak at $q = 7\text{--}15 \text{ nm}^{-1}$ is attributed to the amorphous and crystalline scattering of the backbone nanopore in the membrane, respectively; the peak at $q = 2 \text{ nm}^{-1}$ is due to the ionic cluster in Nafion. Meanwhile, a new peak ($q = 4.0 \text{ nm}^{-1}$) was generated in such a composite membrane. According to the

Equation of $d = 2\pi/q$,^[17] the d value of the new peak is 1.57 nm, which is much close to the characteristic pore size (1.66 nm) in the $\text{NH}_2\text{-GDY}$ (Figure 1i). Thus, it can be deduced that the $\text{NH}_2\text{-GDY}$ causes smaller ionic clusters in Nafion, which is good for suppressing in the methanol crossover.

It is necessary to take measurements to observe the small ionic clusters, which is helpful to understand the interaction between the $\text{NH}_2\text{-GDY}$ and Nafion. Then, the TEM sample was prepared by the precision ion polishing system. Figure 2e shows good continuousness of $\text{NH}_2\text{-GDY}$ in the Nafion matrix, meaning that the $\text{NH}_2\text{-GDY}$ is mechanically stable during the preparation. The magnified image of Figure 2f demonstrates that the $\text{NH}_2\text{-GDY}$ film is about 20 nm, and the color gradually becomes darker close to the $\text{NH}_2\text{-GDY}$. This is due to the induced enrichment of the sulfonic groups by the $\text{NH}_2\text{-GDY}$. It is the evidence that the $\text{NH}_2\text{-GDY}$ interacts intensively with Nafion. Thus, these two components have good compatibility, and during the application, the induced assembly of Nafion will have additional influence in its performance. According to Figure 2g and the Supporting Information, Figure S20, the clear profile of $\text{NH}_2\text{-GDY}$ can be found. The ordered phase separation with a distance of about 1.7 nm is clearly observed in Figure 2h, which is much close to that of two adjacent nanopores, as shown in Figure 2i. Moreover, such value is consistent with the result in the GIXRD test. Accordingly, it can be inferred that the new peak in the GIXRD is ascribed to the ordered assembly of Nafion by $\text{NH}_2\text{-GDY}$. The induced assembly is also certified in the elemental distribution mapping of Figure 2j–m and the Supporting Information, Figures S21, S22. It is found that the

elements of O, S, and F from Nafion are remarkably enriched near the NH₂-GDY, implying their intensive interaction.

Therefore, the assembly of Nafion on NH₂-GDY can be illustrated in Figure 3 a–c. During the preparation, the NH₂-GDY and the Nafion molecules are interlocked together owing to the acid–base interaction, thus the NH₂-GDY plays

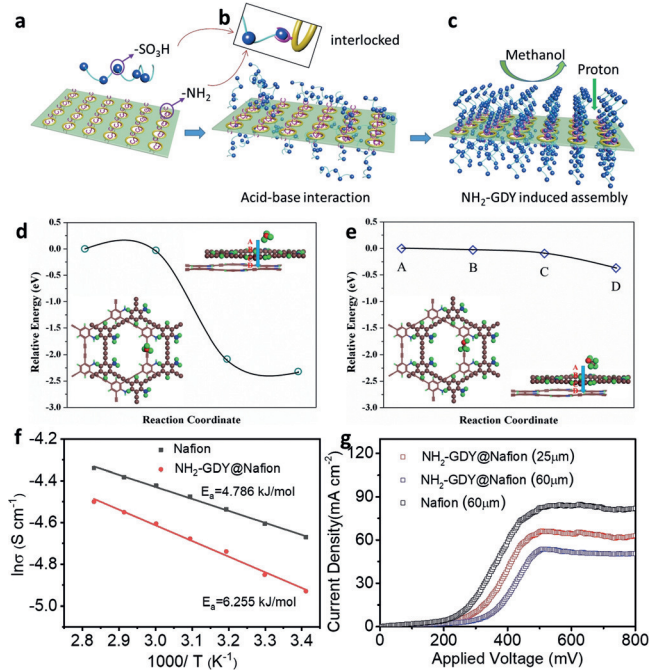


Figure 3. Possible assembly and theoretical simulation. a)–c) Illustrations showing the assembly of Nafion on NH₂-GDY; d), e) the energy variation when the hydrated proton (d) and the methanol molecule (e) passing through NH₂-GDY; f) the temperature dependence of the proton conductivity; g) the methanol crossover current densities at 65 °C in 1 M methanol solution.

as the template for the smaller and ordered ionic clusters, which is good for stopping fuel permeation. Additionally, the native selectivity of NH₂-GDY between the methanol and hydrated proton were also calculated by using the Vienna ab initio simulation package (VASP). The high amount of the sp-hybridized carbon atoms is the unique character of GDY. The optimized configurations (Supporting Information, Figure S23) demonstrate that the sp-hybridized carbon atoms can realize the selectivity between the hydrated proton and the methanol because the hydrated proton has a much higher binding energy of 1.74 eV than that of methanol (0.07 eV). The higher binding energy is ascribed to the charge transfer between the hydrated proton and the sp-hybridized carbon atoms (Supporting Information, Figure S23a). In contrast, there is no obvious charge transfer between the methanol and the NH₂-GDY (Supporting Information, Figure S23b). For simplifying the transport process, one starting position on a two-layer NH₂-GDY film were used as the calculation model (insets in Figure 3 d,e). The design of this model is because this behavior will be repeated in a thick NH₂-GDY film for these molecules. The plots in Figure 3 d,e show the energy variations during the process. When the hydrated

proton moves forward to the diyne linkage, the interaction between the hydrated proton and the diyne linkage is strongly enhanced from 0 to about 2.3 eV. However, it changes very small in the case of the methanol. The big difference demonstrates that the sp-hybridization-carbon-rich channels in the NH₂-GDY are preferential for the accessibility of the hydrated protons (Supporting Information, Figure S24). Accordingly, the NH₂-GDY will be a promising membrane for realizing the selective accessibility of proton and suppressing the methanol permeability.

The NH₂-GDY shows intrinsic selectivity between the methanol and hydrated proton, and it also reduces the size of the nanochannels for the methanol transport in the Nafion matrix owing to the acid–base interaction. Then, the temperature-dependence proton conductivity was tested (Supporting Information, Figures S25, S26). Figure 3 f shows that the conductivity of such composite membrane is slightly lower than the pure Nafion from 25 to 80 °C. It is understandable for this phenomenon because of the selectivity of NH₂-GDY and the smaller ionic cluster near its surface. We can find that the variations of the proton conductivity follows the Arrhenius relationship of $\sigma = \sigma_0 \exp(-E_a/kT)$.^[18] In the equation, the σ is the proton conductivity, the E_a is the activation energy. The slope of the plot in Figure 3 f reveals that the composite membrane has an E_a of 6.255 kJ mol⁻¹, which is slightly higher than the pure Nafion (4.786 kJ mol⁻¹). Besides, the composite membrane has stable mechanical property (Supporting Information, Figure S27). Nafion has excellent proton conductivity, therefore it is cost-efficient if a slight decrease in the conductivity can greatly prevent the methanol crossover. As shown in Figure 3 g, the highest oxidation current density of the pure Nafion is 84.5 mA cm⁻², which is greatly suppressed to 65 and 53 mA cm⁻², respectively in the composite membrane with thickness of 25 and 60 μm. Therefore, this thin NH₂-GDY film efficiently suppresses 23% and 38% methanol permeation. However, in a thicker composite membrane of 90 μm (Supporting Information, Figure S28), it has a current density of 50 mA cm⁻². This shows that the NH₂-GDY film is the main factor for this improvement.

The membrane electrode assembly (MEA) is obtained for the single-cell DMFC (Supporting Information, Figure S29). Figure 4 and the Supporting Information, Figure S30 show the corresponding polarization curves of the DMFC based on these MEAs. For the pure Nafion (60 μm) (Figure 4 a), the cell has an open circuit voltage (OCV) of 0.27, 0.3, 0.33 V at the temperature of 25, 65, 80 °C, respectively. The maximum power density of such cell is increased from 10 (25 °C) to 25 mW cm⁻² (80 °C), because a higher temperature enhances the membrane conductivity and catalytic activity. While using NH₂-GDY@Nafion-25 (Figure 4 b), the performance is obviously higher than that of the plain Nafion. The maximum power output is improved to 11.2 (25 °C), 24.3 (65 °C), and 42.5 mW cm⁻² (80 °C), respectively. It is very promising and attractive that such a high power density can be approached base on the composite membrane with a thickness of 25 μm. Compared with the pure Nafion membrane (60 μm), it saves 58% Nafion and achieves higher performance. Especially in the NH₂-GDY@Nafion-60 (Figure 4 c), the OCV of this single cell is up to 0.54, 0.58, 0.59 V at the temperatures of 25, 65, and

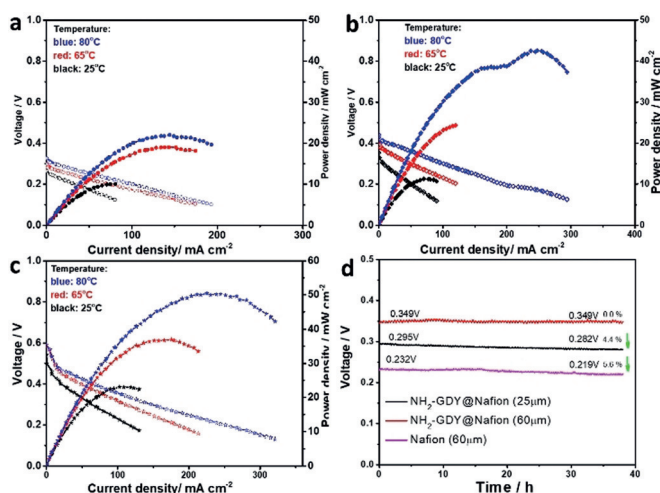


Figure 4. Electrochemical performance. a)–c) Polarization curves and power densities of the DMFCs with Nafion, $\text{NH}_2\text{-GDY@Nafion-25}$, and $\text{NH}_2\text{-GDY@Nafion-60}$, respectively; d) Stability of the DMFCs under current density of 50 mA cm^{-2} . Methanol concentration: 1 M, cell temperature: 65°C .

80°C , respectively. The maximum power density is further increased to $23 (108 \text{ mA cm}^{-2})$, $36.8 (165 \text{ mA cm}^{-2})$, and $50 (225 \text{ mA cm}^{-2}) \text{ mW cm}^{-2}$ at 25, 65, and 80°C , respectively. Indeed, the $\text{NH}_2\text{-GDY@Nafion-60}$ exhibits 2.5 times higher power density than the plain Nafion ($60 \mu\text{m}$) and only about 25% higher than the $\text{NH}_2\text{-GDY@Nafion-25}$. Thus, the increased degree in the power output at 80°C indicates that the performance enhancement is mainly attributed to the introduction of $\text{NH}_2\text{-GDY}$. This phenomenon is further confirmed in the case of $\text{NH}_2\text{-GDY@Nafion-90}$ (Supporting Information, Figure S30), in which only a power density of 59.5 mW cm^{-2} can be approached at 80°C . The long-term stability of all DMFCs is obtained under a current density of 50 mA cm^{-2} . Figure 4d shows that the cell with the $\text{NH}_2\text{-GDY}$ output a more stable and higher voltage after 38 h than that of the pure Nafion. This phenomenon is also ascribed to the lower permeability and the stable interaction between Nafion and $\text{NH}_2\text{-GDY}$.

In summary, the 2D $\text{NH}_2\text{-GDY}$ with well-defined structure is first prepared to realize the good selectivity between the proton and methanol. The DMFCs based on such membrane show improved performance. This work for constructing selective 2D carbon material detours the challenges facing in the perforation technology and thin carbon film preparation. It opens the new way in solving the selective transfer problems in applications of fuel cells, batteries, catalysts, gas separation, purification, and so on.

Acknowledgements

We appreciate the National Natural Science Foundation of China (21790050, 21790051), the National Key Research and Development Project of China (2018YFA0703501), (2016YFA0200104), the Key Program of the Chinese Academy of Sciences (CAS) (QYZDY-SSW-SLH015), and the

Youth Innovation Promotion Association of CAS (2019032), and the National Science Foundation for Young Scientists of China (51802311).

Conflict of interest

The authors declare no conflict of interest.

Keywords: carbon materials · direct methanol fuel cells · graphdiyne · methanol crossover · selective transport

How to cite: *Angew. Chem. Int. Ed.* **2019**, *58*, 15010–15015
Angew. Chem. **2019**, *131*, 15152–15157

- [1] a) T. Ouyang, Y. Q. Ye, C. Y. Wu, K. Xiao, Z. Q. Liu, *Angew. Chem. Int. Ed.* **2019**, *58*, 4923–4928; *Angew. Chem.* **2019**, *131*, 4977–4982; b) X. T. Wang, T. Ouyang, L. Wang, J. H. Zhong, T. Ma, Z. Q. Liu, *Angew. Chem. Int. Ed.* **2019**, *58*, <https://doi.org/10.1002/anie.201907595>; *Angew. Chem.* **2019**, *131*, <https://doi.org/10.1002/ange.201907595>.
- [2] a) N. Kakati, J. Maiti, S. H. Lee, S. H. Jee, B. Viswanathan, Y. S. Yoon, *Chem. Rev.* **2014**, *114*, 12397–12429; b) H. Zhang, P. K. Shen, *Chem. Rev.* **2012**, *112*, 2780–2832.
- [3] D. W. Shin, M. D. Guiver, Y. M. Lee, *Chem. Rev.* **2017**, *117*, 4759–4805.
- [4] R. B. M. Kenneth, A. Mauritz, *Chem. Rev.* **2004**, *104*, 4535.
- [5] a) Y. Li, L. Liang, C. Liu, Y. Li, W. Xing, J. Sun, *Adv. Mater.* **2018**, *30*, 1707146; b) Z. W. Chen, B. Holmberg, W. Z. Li, X. Wang, W. Q. Deng, R. Munoz, Y. S. Yan, *Chem. Mater.* **2006**, *18*, 5669–5675; c) J.-D. Kim, Y. Oba, M. Ohnuma, M.-S. Jun, Y. Tanaka, T. Mori, Y.-W. Choi, Y.-G. Yoon, *J. Electrochem. Soc.* **2010**, *157*, B1872–B1877.
- [6] a) B. G. Choi, J. Hong, Y. C. Park, D. H. Jung, W. H. Hong, P. T. Hammond, H. Park, *ACS Nano* **2011**, *5*, 5167–5174; b) W. Gao, G. Wu, M. T. Janicke, D. A. Cullen, R. Mukundan, J. K. Baldwin, E. L. Brosha, C. Galande, P. M. Ajayan, K. L. More, A. M. Dattelbaum, P. Zelenay, *Angew. Chem. Int. Ed.* **2014**, *53*, 3588–3593; *Angew. Chem.* **2014**, *126*, 3662–3667; c) P. Velayutham, A. K. Sahu, *J. Phys. Chem. C* **2018**, *122*, 21735–21744; d) H. S. Sasmal, H. B. Aiyappa, S. N. Bhange, S. Karak, A. Halder, S. Kurungot, R. Banerjee, *Angew. Chem. Int. Ed.* **2018**, *57*, 10894–10898; *Angew. Chem.* **2018**, *130*, 11060–11064.
- [7] a) Y. Yang, X. Yang, L. Liang, Y. Gao, H. Cheng, X. Li, M. Zou, R. Ma, Q. Yuan, X. Duan, *Science* **2019**, *364*, 1057–1062; b) L. Tsetseris, S. T. Pantelides, *Carbon* **2014**, *67*, 58–63.
- [8] a) Z. Zuo, Y. Li, *Joule* **2019**, *3*, 899–903; b) C. Huang, Y. Li, N. Wang, Y. Xue, Z. Zuo, H. Liu, Y. Li, *Chem. Rev.* **2018**, *118*, 7744–7803.
- [9] a) H. Shang, Z. Zuo, L. Li, F. Wang, H. Liu, Y. Li, Y. Li, *Angew. Chem. Int. Ed.* **2018**, *57*, 774–778; *Angew. Chem.* **2018**, *130*, 782–786; b) Y. Xue, B. Huang, Y. Yi, Y. Guo, Z. Zuo, Y. Li, Z. Jia, H. Liu, Y. Li, *Nat. Commun.* **2018**, *9*, 1460; c) C. Kuang, G. Tang, T. Jiu, H. Yang, H. Liu, B. Li, W. Luo, X. Li, W. Zhang, F. Lu, J. Fang, Y. Li, *Nano Lett.* **2015**, *15*, 2756–2762.
- [10] a) J. Kou, X. Zhou, H. Lu, F. Wu, J. Fan, *Nanoscale* **2014**, *6*, 1865–1870; b) H. Zhang, X. He, M. Zhao, M. Zhang, L. Zhao, X. Feng, Y. Luo, *J. Phys. Chem. C* **2012**, *116*, 16634–16638; c) M. Bartolomei, E. Carmona-Novillo, M. I. Hernández, J. Campos-Martínez, F. Pirani, G. Giorgi, *J. Phys. Chem. C* **2014**, *118*, 29966–29972; d) L. Shi, A. Xu, D. Pan, T. Zhao, *Nat. Commun.* **2019**, *10*, 1165; e) Y. Jiao, A. J. Du, M. Hankel, Z. H. Zhu, V. Rudolph, S. C. Smith, *Chem. Commun.* **2011**, *47*, 11843–11845.
- [11] G. Li, Y. Li, H. Liu, Y. Guo, Y. Li, D. Zhu, *Chem. Commun.* **2010**, 46, 3256–3258.

- [12] X. Gao, Y. Zhu, D. Yi, J. Zhou, S. Zhang, C. Yin, F. Ding, S. Zhang, X. Yi, J. Wang, L. Tong, Y. Han, Z. Liu, J. Zhang, *Sci. Adv.* **2018**, *4*, eaat6378.
- [13] a) J. He, N. Wang, Z. Cui, H. Du, L. Fu, C. Huang, Z. Yang, X. Shen, Y. Yi, Z. Tu, Y. Li, *Nat. Commun.* **2017**, *8*, 1172; b) N. Wang, J. He, Z. Tu, Z. Yang, F. Zhao, X. Li, C. Huang, K. Wang, T. Jiu, Y. Yi, Y. Li, *Angew. Chem. Int. Ed.* **2017**, *56*, 10740–10745; *Angew. Chem.* **2017**, *129*, 10880–10885; c) N. Wang, X. Li, Z. Tu, F. Zhao, J. He, Z. Guan, C. Huang, Y. Yi, Y. Li, *Angew. Chem. Int. Ed.* **2018**, *57*, 3968–3973; *Angew. Chem.* **2018**, *130*, 4032–4037.
- [14] C. T. Wolke, J. A. Fournier, L. C. Dzigan, M. R. Fagiani, T. T. Odbadrakh, H. Knorke, K. D. Jordan, A. B. McCoy, K. R. Asmis, M. A. Johnson, *Science* **2016**, *354*, 1131–1135.
- [15] K. Xu, *Nat. Energy* **2019**, *4*, 93–94.
- [16] M. Fujimura, T. Hashimoto, H. Kawai, *Macromolecules* **1982**, *15*, 136–144.
- [17] J. Halim, G. G. Scherer, M. Stamm, *Macromol. Chem. Phys.* **1994**, *195*, 3783–3788.
- [18] X. Liu, Y. Li, J. Xue, W. Zhu, J. Zhang, Y. Yin, Y. Qin, K. Jiao, Q. Du, B. Cheng, X. Zhuang, J. Li, M. D. Guiver, *Nat. Commun.* **2019**, *10*, 842.

Manuscript received: August 19, 2019

Accepted manuscript online: September 3, 2019

Version of record online: September 13, 2019